IEEE Open Journal of
Industry Applications

Received 7 October 2020; revised 28 November 2020; accepted 10 December 2020. Date of publication 14 December 2020; date of current version 4 January 2021. The review of this article was arranged by Associate Editor Luca Solero.

Digital Object Identifier 10.1109/OJIA.2020.3044810

Decentralised Optimal Controller Design of Variable Frequency Three-Phase Power Electronic Networks Accounting for Sub-System Interactions

DAVID DEWAR [1] (Student Member, IEEE), JAIME ROHTEN [2] (Member, IEEE), ANDREA FORMENTINI [1] (Member, IEEE), AND PERICLE ZANCHETTA [1] (Fellow, IEEE)

(Invited Paper)

[1] Electrical and Electronic Engineering, University of Nottingham, Nottingham NG7 2RD, U.K.
[2] Department of Electrical Engineering, Universidad del Bio Bio, Concepción 3349001, Chile

CORRESPONDING AUTHOR: DAVID DEWAR (e-mail: eexdnd@nottingham.ac.uk)

ABSTRACT Electrification of non-propulsive aircraft systems has resulted in the increased proliferation of power electronics embedded grids on aircraft. Typically, power converters on these networks are optimised locally without consideration to the wider grid dynamics, which as a result increases the interactive effect between sub-systems. Filters are typically used to decouple these interactive effects, however since weight is a key design factor for aircraft, filters are typically reduced in size, further increasing interactive effects. Recent studies into H_2 control, due to its ability to develop decentralised controls whilst considering the global grid dynamic model, have shown to reduce these interactive effects, however studies concentrate only on fixed frequency systems, atypical to modern variable frequency grids on modern aircraft today. In this paper, H_2 optimisation is used to optimise a target converter to a pre-designed converter generating the variable frequency AC bus. The proposed method shows that not only are interactions reduced on the target converter for all frequencies but allows the pre-designed system to run as designed without detrimental performance, even during large power transients for full range of frequencies. This paper includes mathematical derivations, key design points, and has been validated and compared against other popular controls by experiment.

INDEX TERMS Decentralised control, optimal control, variable frequency, non-linear system, more electric aircraft.

I. INTRODUCTION

Recently, modern civil aircraft have made significant changes to their non-propulsive power utilization. The heavy, and generally unreliable pneumatic, hydraulic and mechanical systems have, over the years, been replaced with more reliable, lighter and cheaper to maintain electrical alternatives. This shift in power utilization of modern aircraft has given rise to the term More Electric Aircraft (MEA) [1]. On traditional aircraft, the main AC bus typically operates at a fixed frequency of 400 Hz. In Modern MEAs however, a variable frequency architecture is often used, operating between 360–800 Hz [2]. This approach allows the elimination of heavy mechanical couplings, which were used to maintain the generators at a constant frequency, whilst the jet engines operate at variable speed, greatly reducing overall weight, and increasing overall efficiency of these aircraft [3], [4]. Due to this, variable frequency systems, also widely known as frequency-wild, have now become the new norm in electrical power transmission in modern day civil aircraft, such as the Boeing 787, and the Airbus A350, and is becoming of interest across alternate kinds of micro-grid networks [5]. With the increasing prevalence of power electronic embedded grids on aircraft, so has the

research interests towards the design, control and optimisation of power converters connected to such sources [6], [7]. Generally, these power electronic networks consist of power converters which have filters interfaced between one another. These filters can contribute upwards of 25–40% of the total weight of the electrical system [8]. Therefore, in the case of aircraft, where the reduction in weight of the electrical system is of paramount importance, filters are generally reduced in size. However, these filters not only have the purpose of filtering out the switching harmonics, but also have the effect of reducing cross-interactions between sub-systems. In the presence of reduced filters, dynamic interactions between sub-systems become more pronounced, and therefore are no longer negligible [9]. In addition, when developing controls for such systems, distributed or decentralised control approaches are favoured with the later preferred since it reduces communications between sub-systems and consequently the size of these systems [10], [11].

As the control synthesis of fully decentralised systems are considered NP-hard (non-deterministic polynomial-time) problems, not much research has been conducted investigating decentralised control systems in MEA applications, and tackling the problem of sub-system interactions in such control architectures [10]. Needless to say, there have been some attempts to develop decentralised control schemes to counteract interactive effects between converters. For instance in [12], the authors approached this by synthesising a collection of alternate independent controllers for each sub-system, and from this find the best combination of controllers which reduce interactive effects between sub-systems the most. Whilst this methodology was shown to attain positive results, there is plenty of room for improvement on this method. Several works have also utilised distributed Model Predictive Controls for grid applications [13]–[15]. Though good at actively damping against harmonic effects due to the filters [14], counteracting against sub-system interactions requires measurements of converters outside the local scope of each decentralised controller, thus requiring additional communication. Therefore, such controllers, in a fully decentralised form can only be optimal on the local level, and not at the global level as required for interaction mitigation [16]. Other papers investigated the use of H_∞ optimal control [17], [18], however, due to the conservativeness of these kinds of control methods, it can be very hard to develop block diagonal structured decentralised controllers, with solutions tending to be sub-optimal. Optimal solutions are only realistically achievable if block diagonal clusters of systems are augmented, requiring communication between converter clusters in order to account for interactions [19]. H_2 control had therefore been used, which is less conservative than H_∞, at the cost of reduced robustness. It was shown in [20], [21] that H_2 does allow for an optimal, and fully decentralised control for the power network. In addition, since the H_2 optimisation uses the whole system model for the development of decentralised controllers, each independent controller is optimised with the knowledge of every other converters closed loop dynamics, and cross-coupled interactive effects. Due to this, studies have shown that this type of controller optimisation largely counteracts coupled interactions between converters [22]. The above studies show that full decentralisation with the capability of mitigating sub-system interactions is possible, however they all assume fixed frequency operation of the grid. These controllers are also optimised about a linearised state-space model, and thus the controller is valid only for a limited area of state-deviation, and thus will not be optimal or even guaranteed to be stable as the operational frequency changes.

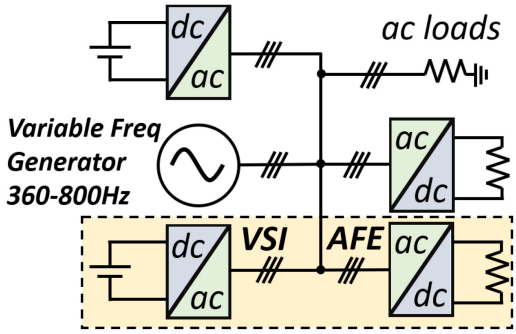

FIGURE 1. The notional variable frequency system under analysis.

This paper delivers two novel contributions. The first is deriving a gain-scheduled decentralised H_2 controller approach to account for system frequency variation. Inspiration can be derived from [23] where variable frequency gain scheduled LQR controls were derived for the linear voltage source inverter (VSI). It will be shown here, given that the H_2 optimisation is non-convex by nature, and the global system being intrinsically non-linear, a smooth polynomial based controller $K(\omega)$ can be developed which not only ensures the optimal performance of the network across the full AC bus operable frequency range of 360–800 Hz, but is also able to retain mitigation of sub-system interactions across this range too. The controller will be shown to be non-computationally heavy and capable of fast dynamic changes to state and frequency. Secondly, this paper presents a methodology for optimising a single converter to a wider pre-designed network. In the studies presented in [20] it was assumed that all parameters of the grid were known and accessible. However, in industrial settings, this is not a likely occurrence. Therefore, the variable frequency based H_2 controller will be applied only to a single converter, which will be optimised with respect to the rest of the electrical system. It will be shown that not only does the optimised converter have superior performance over traditionally control schemes, but also allows the pre-designed converter with its controller to operate as designed, without any performance degradation, thanks to the interaction mitigation intrinsic to the proposed H_2 decentralised controller.

II. NOTIONAL SYSTEM MODEL

This work studies the case of a variable frequency electrical distribution system as depicted in Fig. 1. For simplification

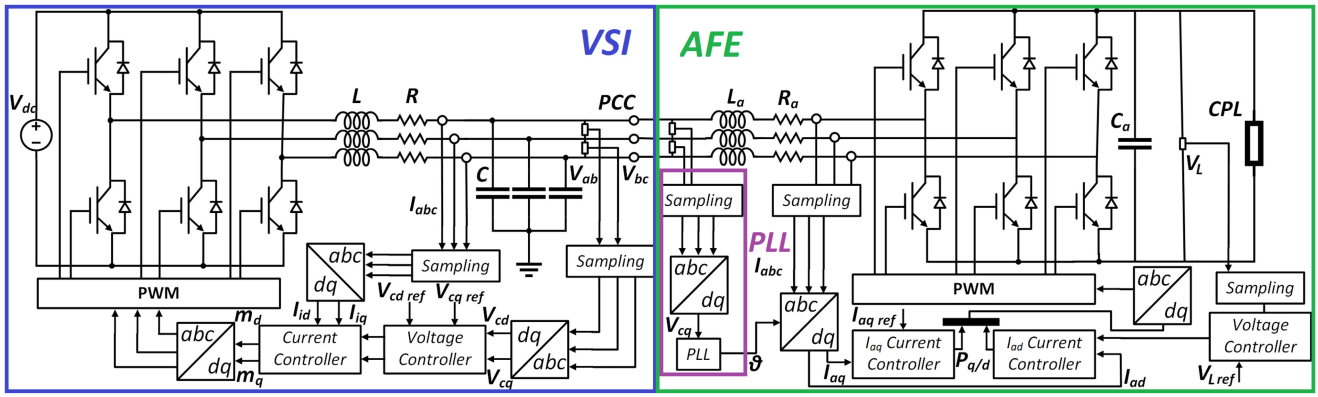

FIGURE 2. Notional system with traditional control scheme for VSI and AFE.

of this analysis a sub-section of the grid will be analysed. A Voltage Source Inverter (VSI) is fed from a fixed DC source, and directly generates the variable frequency grid, on the assumption that grid frequency is known to the VSI controller. An output LCR filter is implemented onto the output terminals of the VSI, and the Active Front End (AFE) which is interfaced with an input LR filter is connected directly to the grid at the point of common coupling (PCC). In this study, the the DC side of the AFE will be interfaced with a constant power load (CPL). These loads are kept to a constant value even when the DC voltage fluctuates. Since the product of the voltage and current must remain constant in a CPL, if the voltage increases/decreases, the current therefore needs to decrease/increase. This behaviour results in a negative incremental impedance characteristic onto the AFE which can have destabilising effects of the rest of the electrical system [24]. The use of the CPL is therefore used to exaggerate the non-linearities of the system to better observe how the proposed controller performs in highly non-linear situations against other forms of controller design.

When dealing with frequency-dependent systems, they are often remodeled in terms of the rotating dq domain. In doing this an individual three-phase converter can be remodelled as two coupled DC systems. Therefore, DC-based controls, which in general are simpler to design and better understood can be employed [20].

A. VSI dq MODEL

Conducting the model transformation detailed in [25] on the configuration represented in Fig. 2, the VSI state equations are:

$$\dot{I}_{id} = -\frac{R}{L}I_{id} - \frac{1}{L}V_{cd} + \omega I_{iq} + \frac{m_d}{2L}V_{dci} \tag{1}$$

$$\dot{V}_{cd} = \frac{1}{C}I_{id} + \omega V_{cq} - \frac{1}{C}I_{ad} \tag{2}$$

$$\dot{I}_{iq} = -\omega I_{id} - \frac{R}{L}I_{iq} - \frac{1}{L}V_{cq} + \frac{m_q}{2L}V_{dci} \tag{3}$$

$$\dot{V}_{cq} = -\omega V_{cd} + \frac{1}{C}I_{iq} - \frac{1}{C}I_{aq} \tag{4}$$

The terms I_{id} and I_{iq} refer to the dq axis currents across the output inductor L, where R is the inductors intrinsic resistance. V_{cd} and V_{cq} refer to the dq axis voltages across the filter capacitors C. I_{ad} and I_{aq} are the output currents of the grid at the PCC going to the AFE. Terms m_d and m_q refer to the dq axis modulation indexes and finally V_{dci} refers to the fixed DC source voltage to the VSI.

B. AFE dq MODEL

The AFE state space equations can be derived from Fig. 2 when loaded with a CPL is as follows:

$$\dot{I}^P_{ad} = \frac{1}{L_a}V^P_{cd} - \frac{R_a}{L_a}I^P_{ad} + \omega I^P_{aq} - \frac{p_d}{2L_a}V_L \tag{5}$$

$$\dot{I}^P_{aq} = \frac{1}{L_a}V^P_{cq} - \omega I^P_{ad} - \frac{R_a}{L_a}I^P_{aq} - \frac{p_q}{2L_a}V_L \tag{6}$$

$$\dot{V}_L = \frac{3}{4C_a}(I^P_{ad}p_d + I^P_{aq}p_q) - \frac{P_l}{C_aV_L} \tag{7}$$

Where I^P_{ad} and I^P_{aq} are the dq output currents from the VSI, and thus the currents across the input filter inductor L_a, with R_a being the inductors intrinsic resistance. V_L is the voltage across the DC-Link capacitor C_a. The terms p_d and p_q refer to the modulation indexes in dq frame, and finally, P_l refers to power demand from the CPL when loaded. The superscript ^{P} defines terms as observed on the PLL dq frame, and shall be further explained in Section II-C. The non-linear system described in (5)–(7) contains two equilibrium points as defined in (8)–(10) [20]:

$$p_d = \frac{V_{cd} \pm \sqrt{V^2_{cd} - \frac{8P_lRa}{3}}}{V_L} \tag{8}$$

$$p_q = -\frac{L_a\omega V_{cd} \mp \sqrt{V^2_{cd} - \frac{8P_lRa}{3}}}{R_aV_L} \tag{9}$$

$$I_{ad} = \frac{V_{cd} \mp \sqrt{V^2_{cd} - \frac{8P_lRa}{3}}}{2R_a} \tag{10}$$

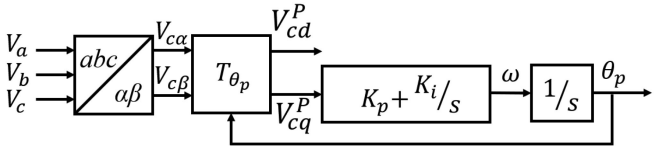

FIGURE 3. Synchronous reference frame PLL block diagram.

Of these two points, one of them can result in an I_{ad} equilibrium of tens to hundred of amps, outside the normal capabilities of most low power converters. On the other hand, the other point results in a lower, more realistic value of current, and thus this smaller current shall be used hereafter for the remainder of the study. The grid voltages are controlled directly by controlling the dq voltages outputted from the VSI, where the d-axis controls the peak to peak 3-phase voltage and the q-axis represents the reactive component. To achieve unity power factor, VSI q-axis voltage is controlled to zero. Similarly, AFE q-axis current is controlled to 0 A. Generally, the AC grid would nominally be at $230V_{rms}$ in aircraft, but due to limitations of the experimental rig, in this work it has been set to $100V_{rms}$. As a proof of concept of the to be proposed controller design, this is deemed an acceptable change.

C. PHASE-LOCKED LOOP dq MODEL

The PLL is a fundamental sub-system responsible in ensuring good power delivery when a converter is connected to an AC bus. In this work a Synchronous Reference Frame PLL (SRF-PLL) has been used to synchronise the AFE to the grid and its block diagram is shown in Fig. 3. The PLL is well discussed in the literature [20], [26] and therefore shall not be described here, however since it is part of the whole global system, its dynamics must be incorporated into the optimisation, and therefore its state-space model must be derived.

From Fig. 3 the SRF-PLL dynamic equation can be attained to be:

$$\begin{bmatrix} V_{cd}^P \\ V_{cq}^P \end{bmatrix} = T_{\theta_P} \begin{bmatrix} V_{c\alpha} \\ V_{c\beta} \end{bmatrix} = \begin{bmatrix} \cos(\theta_P) & \sin(\theta_P) \\ -\sin(\theta_P) & \cos(\theta_P) \end{bmatrix} \begin{bmatrix} V_{c\alpha} \\ V_{c\beta} \end{bmatrix} \quad (11)$$

Where the term θ_P denotes the estimated angle of the grid, and the transformation T_{θ_P} is a transformation of the $\alpha\beta$ voltages into the dq frame using θ_P as the angle of the dq reference frame. As mentioned earlier, the terms subscripted ^{p} are quantities on the PLL dq reference frame, which is the what the AFE uses, and is generated from the estimated angle θ_P of the PLL. Additionally from Fig. 3, the following control equations can be derived

$$\dot{\theta}_P = K_{P_{pll}}(-\sin(\theta_P)V_{c\alpha} + \cos(\theta_P)V_{c\beta}) + \Psi \quad (12)$$

$$\dot{\Psi} = K_{I_{pll}}(-\sin(\theta_P)V_{c\alpha} + \cos(\theta_P)V_{c\beta}) \quad (13)$$

The terms $K_{P_{pll}}$ and $K_{I_{pll}}$ define the proportional and integral gains of the PLL, and Ψ defines the PLL's integral state. Additionally, since it is expected that the grid angle should be tracked accurately by the PLL with only small error during transients, it becomes easier to model the dynamic equations

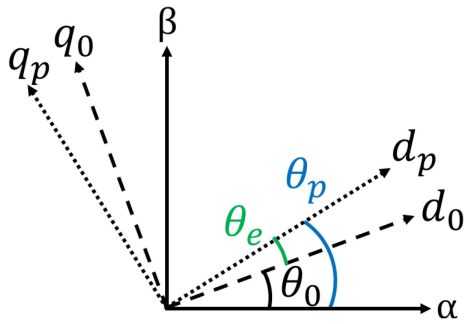

FIGURE 4. Angle representation of the real grid phase θ_0, PLL predicted phase angle θ_P and the angle error θ_e.

of the system in terms of the angle error θ_e between the real grid phase generated by the VSI, θ_0, and PLL estimated grid angle, where Fig. 4 shows the relation between each of these quantities.

$$\theta_e := \theta_p - \theta_0 \Rightarrow \theta_p = \theta_e + \theta_0 \quad (14)$$

To model the PLL in terms of θ_e, one can use the notion that as VSI $\alpha\beta$ voltages rotates the VSI dq frame, θ_e is the rotational difference between θ_P and θ_0. Since the VSI states V_{cd} and V_{cq} are controlled to 100 V and 0 V respectively, it will be known that true alignment of the PLL to the grid has occurred once the PLL dq-frame voltages equate exactly to the dq reference voltages of the VSI. Thus, if $V_{cd}^P \neq V_{cd}$ and $V_{cq}^P \neq V_{cq}$, then any error between these values can be attributed directly to θ_e. Assuming the error between the frames remains small, one can therefore translate (12) and (13) in terms of angle error between the two dq frames, such that:

$$\dot{\theta}_e = -K_{P_{pll}}\sin(\theta_e)V_{cd} + K_{P_{pll}}\cos(\theta_e)V_{cq} + \Psi + \omega_0 \quad (15)$$

$$\dot{\Psi} = -K_{I_{pll}}\sin(\theta_e)V_{cd} + K_{I_{pll}}\cos(\theta_e)V_{cq} \quad (16)$$

where the term ω_0 represents the nominal grid frequency, which for aircraft is typically set to 400 Hz. This is only necessary during the implementation phase of the controller, and as such, can be dropped for the remainder of the analysis. At this point, equations (15) and (16) can be linearised about the known steady-state equilibrium point of $\theta_e^* = 0, V_{cq}^* = 0$, and V_{cd}^* set to the VSI V_{cd} reference voltage, providing the final control equation in state-space form:

$$\dot{\theta}_e = -K_{P_{pll}}V_{cd}^*\theta_e + K_{P_{pll}}V_{cq}^* + \Psi \quad (17)$$

$$\dot{\Psi} = -K_{I_{pll}}V_{cd}^*\theta_e + K_{I_{pll}}V_{cq}^* \quad (18)$$

Where $*$ defines states at their equilibrium positions. The presence of two alternate dq-frames in this system therefore leads to the need to transform each of the cross-coupling terms to their converter respective dq-frames. For instance, the AFE states defined in (5) and (6), are dependant on V_{cd}^P and V_{cq}^P respectively being correctly aligned with the grid generating VSI voltages V_{cd} and V_{cq}. If misalignment between frames is present, as per Fig. 4, VSI voltages in the PLL frame are then observed to be rotated by θ_e. Modelling this difference can be performed using the same transformation in (11) but instead

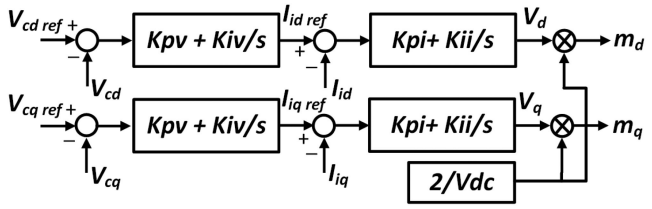

FIGURE 5. VSI PI control block diagram.

submitting θ_e as the rotation angle, such that:

$$\begin{bmatrix} V_{cd}^P \\ V_{cq}^P \end{bmatrix} = T_{\theta_e} \begin{bmatrix} V_{cd} \\ V_{cq} \end{bmatrix} = \begin{bmatrix} \cos(\theta_e) & \sin(\theta_e) \\ -\sin(\theta_e) & \cos(\theta_e) \end{bmatrix} \begin{bmatrix} V_{cd} \\ V_{cd} \end{bmatrix} \tag{19}$$

Resulting in the definitions of the terms V_{cd}^P and V_{cq}^P being rewritten as:

$$\begin{aligned} V_{cd}^p &= V_{cd}\cos(\theta_e) + V_{cq}\sin(\theta_e) \\ V_{cq}^p &= -V_{cd}\sin(\theta_e) + V_{cq}\cos(\theta_e) \end{aligned} \tag{20}$$

Similarly, the VSI states (2) and (4) are dependant on the correct alignment of the AFE for the currents I_{ad} and I_{aq}. Since from Fig. 4, we're assuming the VSI is of a rotation of $-\theta_e$ when compared to the AFE, an inverse of the transformation performed in (19) can be done to rewrite the terms I_{ad} and I_{aq} as:

$$\begin{aligned} I_{ad} &= I_{ad}^p\cos(\theta_e) - I_{aq}^p\sin(\theta_e) \\ I_{aq} &= I_{ad}^p\sin(\theta_e) + I_{aq}^p\cos(\theta_e) \end{aligned} \tag{21}$$

These redefined terms, (20) and (21), become important later in Section III-B when incorporating the effect of PLL interactions into the state-space model.

III. GLOBAL SYSTEM MODEL

As previously mentioned, the goal is to develop an optimal controller for a to-be-designed AFE sub-system with regards to the rest of the embedded aircraft system. Since the VSI is separately designed, in order to accurately optimise the AFE, the closed loop equations of the VSI must be provided to the optimisation for the AFE tuning process. This shall be shown in the next section.

A. CLOSED LOOP VSI STATE-SPACE MODEL

For the control of VSIs, the most commonly employed and well understood control schemes is the cascaded PI, as shown in Fig. 5.

To encapsulate the closed loop dynamics of the VSI into the global system model, the VSI state-space equation can be extended by four additional states. Each state defined by each of the outputs of the cascade PI control.

$$\dot{\Lambda}_{dp} = -K_{pv}\dot{V}_{cd} + K_{iv}(V_{cd_{ref}} - V_{cd}) \tag{22}$$

$$\dot{\Lambda}_{qp} = -K_{pv}\dot{V}_{cq} + K_{iv}(V_{cq_{ref}} - V_{cq}) \tag{23}$$

$$\dot{\Lambda}_{d} = K_{pi}(\dot{\Lambda}_{dp} - \dot{I}_{id}) + K_{ii}(\Lambda_{dp} - I_{id}) \tag{24}$$

$$\dot{\Lambda}_{q} = K_{pi}(\dot{\Lambda}_{qp} - \dot{I}_{iq}) + K_{ii}(\Lambda_{qp} - I_{iq}) \tag{25}$$

Where K_{pv} and K_{iv} are the proportional and integrals gains for the voltage control, and likewise K_{pi} and K_{ii} for the current controllers. The terms Λ_{dp} and Λ_{qp} being the output of the outer voltage PI controller, and Λ_d and Λ_q the outputs for the inner current controller for the d and q axis respectively.

The terms (1)–(4) in conjunction with (22)–(25) forms the global state space equation for the VSI. With the states Λ_d and Λ_q being the final resultant action of the controller, these terms need to be properly attributed into the open loop VSI equations. From the control block diagram in Fig. 5, this can be performed by the simple redefinition of the modulation index terms and this transformation will be carried forward for the rest of this study.

$$\frac{m_d V_{dci}}{2} = \Lambda_d \quad \frac{m_q V_{dci}}{2} = \Lambda_q \tag{26}$$

B. INCORPORATION OF PLL INTERACTIVE BEHAVIOUR

At steady state, the VSI and PLL dq-frame angles should be equal, resulting in $\theta_e = 0$, and thus cross-coupled terms between converters being equivalent. However, as previously discussed, if $\theta_e \neq 0$, then this results in the dq-frames of the converter sub-systems to become misaligned. Since, both the VSI and AFE have cross-coupling terms in their state-equations, misalignment of the PLL to the grid, can cause interactive effects between both sub-systems. Equations (20) and (21) presented how each of the cross-coupling terms found in each converter's state equations can be redefined, as to attribute the angle θ_e of misalignment between the two converters dq-frames during disturbance events. Therefore, by substituting (20) into the AFE state equations (5) and (6), where cross-coupling with VSI is present, the states can then be defined as those in (27) and (28) respectively, to correctly account for misaligned cross-coupled VSI states in the AFE model.

$$\begin{aligned} \dot{I}_{ad}^P = &-\frac{R_a}{L_a}I_{ad}^P + \omega I_{aq}^P - \frac{p_d}{2L_a}V_L \\ &+ \frac{1}{L_a}\left(V_{cd}\cos(\theta_e) + V_{cq}\sin(\theta_e)\right) \end{aligned} \tag{27}$$

$$\begin{aligned} \dot{I}_{aq}^P = &-\omega I_{ad}^P - \frac{R_a}{L_a}I_{aq}^P - \frac{p_q}{2L_a}V_L \\ &+ \frac{1}{L_a}\left(-V_{cd}\sin(\theta_e) + V_{cq}\cos(\theta_e)\right) \end{aligned} \tag{28}$$

Similarly, in the VSI state equations (2) and (4) include AFE cross-coupling terms I_{ad} and I_{aq}. To correctly model these cross-coupled terms in events of frame misalignment, one can substitute (21) into these state equations in order to derive redefined VSI state-space equations taking into account PLL interactions:

$$\dot{V}_{cd} = \frac{1}{C}I_{id} + \omega V_{cq} - \frac{1}{C}\left(I_{ad}\cos(\theta_e) - I_{aq}\sin(\theta_e)\right) \tag{29}$$

$$\dot{V}_{cq} = -\omega V_{cd} + \frac{1}{C}I_{iq} - \frac{1}{C}\left(I_{ad}\sin(\theta_e) + I_{aq}\cos(\theta_e)\right) \tag{30}$$

Note additionally, that with (29) and (30) redefining the VSI state-space model, these terms must also be submitted

into (22) and (23) respectively to ensure the closed loop PI controller states of the VSI are correctly modelled accounting for PLL interactions.

C. FORMULATION OF THE GLOBAL MODEL

VSI, AFE and PLL equations can be merged resulting in

$$\dot{x} = Ax + B_2 u \tag{31}$$

where A is the state-matrix, B_2 the control input matrix and x and u are the state and input vectors respectively, and are defined as follows:

$$x = \begin{bmatrix} x_{vsi} \; x_{afe} \; x_{pll} \end{bmatrix}^T \tag{32}$$

$$x_{vsi} = \begin{bmatrix} I_{id} \; V_{cd} \; I_{iq} \; V_{cq} \; \Lambda_{dp} \; \Lambda_d \; \Lambda_{qp} \; \Lambda_q \end{bmatrix} \tag{33}$$

$$x_{afe} = \begin{bmatrix} I^P_{ad} \; I^P_{aq} \; V_L \; \chi_{I_{aq}} \; \chi_{V_L} \end{bmatrix} \tag{34}$$

$$x_{pll} = \begin{bmatrix} \theta_e \; \Psi \end{bmatrix} \tag{35}$$

$$u = \begin{bmatrix} p_d \; p_q \end{bmatrix}^T \tag{36}$$

Because the AFE in this study is the only converter which will be optimized, only AFE inputs have been defined in u.

States in x denoted χ are integral states to their sub-scripted terms. They are present in the AFE controller implementation in order to ensure zero steady-state error on the critical control states. The terms A and B_2 from (31) are defined as

$$A = \begin{bmatrix} A_{vsi_{cl}} & A_{C_v} & A_{P_v} \\ A_{C_a} & A_{afe} & A_{P_a} \\ A_{V_p} & A_{A_p} & A_{pll} \end{bmatrix}, B_2 = \begin{bmatrix} \mathbf{0}^{8\times 2} \\ -\frac{V_L}{2L_a} \quad 0 \\ 0 \quad -\frac{V_L}{2L_a} \\ \frac{3I_{ad_{pll}}}{4C_a} \quad \frac{3I_{aq_{pll}}}{4C_a} \\ \mathbf{0}^{4\times 2} \end{bmatrix} \tag{37}$$

$$A_{vsi_{cl}} = \begin{bmatrix} -\frac{R}{L} & -\frac{1}{L} & \omega & 0 & 0 & 0 & 0 & 0 \\ \frac{1}{C} & 0 & 0 & \omega & 0 & 0 & 0 & 0 \\ -\omega & 0 & -\frac{R}{L} & -\frac{1}{L} & 0 & 0 & 0 & 0 \\ 0 & -\omega & -\frac{1}{C} & 0 & 0 & 0 & 0 & 0 \\ -\frac{K_{pv}}{C} & -K_{iv} & 0 & -K_{pv}\omega & 0 & 0 & 0 & 0 \\ -K_{ii}+\sigma_1 & \sigma_2 & -K_{pi}\omega & \sigma_3 & K_{ii} & 0 & 0 & 0 \\ 0 & K_{pv}\omega & \frac{K_{pv}}{C} & -K_{iv} & 0 & 0 & 0 & 0 \\ K_{pi}\omega & -\sigma_3 & -K_{ii}-\sigma_1 & \sigma_2 & 0 & K_{ii} & 0 & 0 \end{bmatrix} \tag{38}$$

$$A_{C_v} = \begin{bmatrix} 0 & 0 & 0 & 0 & 0 \\ -\frac{1}{C} & 0 & 0 & 0 & 0 \\ 0 & 0 & 0 & 0 & 0 \\ 0 & -\frac{1}{C} & 0 & 0 & 0 \\ \frac{K_{pv}}{C} & 0 & 0 & 0 & 0 \\ \frac{K_{pi}K_{pv}}{C} & 0 & 0 & 0 & 0 \\ 0 & \frac{K_{pv}}{C} & 0 & 0 & 0 \\ 0 & \frac{K_{pi}K_{pv}}{C} & 0 & 0 & 0 \end{bmatrix} \tag{39}$$

$$A_{P_v} = \begin{bmatrix} 0 & 0 \\ -\frac{I_{aq}}{C} & 0 \\ 0 & 0 \\ \frac{I_{ad}}{C} & 0 \\ \frac{I_{aq}K_{pv}}{C} & 0 \\ \frac{I_{aq}K_{pi}K_{pv}}{C} & 0 \\ -\frac{I_{ad}K_{pv}}{C} & 0 \\ -\frac{I_{ad}KpiK_{pv}}{C} & 0 \end{bmatrix} \tag{40}$$

$$A_{C_a} = \begin{bmatrix} 0 & \frac{2}{L_a} & 0 & 0 & \\ 0 & 0 & 0 & \frac{2}{L_a} & \\ 0 & 0 & 0 & 0 & \mathbf{0}^{5\times 4} \\ 0 & 0 & 0 & 0 & \\ 0 & 0 & 0 & 0 & \end{bmatrix} \tag{41}$$

$$A_{afe} = \begin{bmatrix} -\frac{R_a}{L_a} & \omega & -\frac{p_d}{2L_a} & 0 & 0 \\ -\omega & -\frac{R_a}{L_a} & -\frac{p_q}{2L_a} & 0 & 0 \\ \frac{3p_d}{4C_a} & \frac{3p_q}{4C_a} & \frac{P_l}{C_a V_L^{*2}} & 0 & 0 \\ 0 & -1 & 0 & 0 & 0 \\ 0 & 0 & -1 & 0 & 0 \end{bmatrix} \tag{42}$$

$$A_{P_a} = \begin{bmatrix} -\frac{V_{cq}}{La} & 0 \\ \frac{V_{cd}}{L_a} & 0 \\ \mathbf{0}^{3\times 2} \end{bmatrix} \tag{43}$$

$$A_{V_p} = \mathbf{0}^{2\times 8} \tag{44}$$

$$A_{A_p} = \mathbf{0}^{2\times 5} \tag{45}$$

$$A_{pll} = \begin{bmatrix} -K_{P_{pll}} V^*_{cd} & 0 \\ -K_{I_{pll}} V^*_{cd} & 0 \end{bmatrix} \tag{46}$$

where all terms of A are defined in matrices (38)–(46) on the next page, where the terms $\sigma_{\langle 1,2,3\rangle}$ found in (38) are defined as:

$$\sigma_1 = -K_{pi}\left(\frac{K_{pv}}{C} - \frac{R}{L}\right) \tag{47}$$

$$\sigma_2 = -K_{pi}\left(K_{iv} - \frac{1}{L}\right) \tag{48}$$

$$\sigma_3 = -K_{pi}K_{pv}\omega \tag{49}$$

IV. SYNTHESIS OF THE OPTIMAL DECENTRALIZED VARIABLE FREQUENCY CONTROLLER

This study looks to optimize a local controller for a grid-tied converter, with respect to the global system dynamics. Controller optimization has been a popular topic in recent researches, for instance the increased adoption of Model Predictive Controls (MPC) [27]. However, such optimization approaches are computationally heavy since they require online optimisation, and are thus not easily scalable to expanding systems. In light of such issues, a H_2 decentralized optimal controller was selected for this study since the H_2 controller

has been popular offline optimization method for embedded grid applications in recent years in order to optimize individual converter controllers all whilst keeping in consideration dynamic interactions between sub-systems [16], [28].

A. OPTIMAL H_2 CONTROL PROBLEM

The proposed H_2 approach takes its origins from the Linear Quadratic Regulator (LQR), whereby the optimal controller is the result of an optimization of a cost function of the form:

$$\min_u \left(\frac{1}{2} \int_0^\infty x(t)^T Q_\gamma x(t) + u(t)^T R_\gamma u(t) dt \right) \tag{50}$$

The terms Q_γ and R_γ are a positive semidefinite state diagonal weighing matrix, and a positive definite diagonal input weighting matrix respectively. The resulting control action is in the form:

$$u = Kx \tag{51}$$

Whilst the LQR approach is well known to offer good dynamic performances and has been shown to be very robust, it requires full state feedback, i.e. matrix K is in general full. This implies that, even if designing considering only the AFE control inputs, the AFE will be totally dependant on all the global system states for good performance of the control. This would require lots of communication between all system converters for the AFE to have optimal operation. This is undesired as this would increase the cost and complexity of the implementation of this controller. This could be solved however, if the problem in (50) is reformulated in order to search directly for the feedback matrix K with an imposed structure on only the AFE states. As such, an optimal controller K for the AFE, with respect to the rest of the system can be generated. This cannot be performed in the standard LQR optimization, however reformulating the problem as a H_2 control problem makes this possible.

Consider the system as described from [29]:

$$\begin{cases} \dot{x}(t) = Ax(t) + B_1 w(t) + B_2 u(t) \\ z(t) = C_1 x(t) + D_{12} u(t) \\ y(t) = C_2 x(t) \end{cases} \tag{52}$$

where w and z represent plant disturbances and performance output respectively. B_1 is the disturbance input matrix and is set to an identity matrix in this work. C_2 is the measured output matrix, where a 1 is provided in the diagonal if that attributed state is accessible for the controller. Since only the AFE states can be provided to the controller for measurement, the C_2 matrix becomes:

$$C_2 = \begin{bmatrix} \mathbf{0}^{8\times 8} & & \\ & I^{5\times 5} & \\ & & \mathbf{0}^{2\times 2} \end{bmatrix} \tag{53}$$

C_1 and D_{12} are the matrices that weight the states and inputs effect on the performance output and are defined as:

$$C_1 = \begin{bmatrix} \sqrt{Q_\gamma} \\ \mathbf{0} \end{bmatrix}, \quad D_{12} = \begin{bmatrix} \mathbf{0} \\ \sqrt{R_\gamma} \end{bmatrix} \tag{54}$$

The H_2 control problem can be defined as:

$$\min_K \|T_{zw}\|_2 \tag{55}$$

where

$$\|T_{zw}\|_2 = tr\left(B_1' \int_0^\infty e^{(A-B_2K)'t} (Q_\gamma + K' R_\gamma K) e^{(A-B_2K)t} dt B_1 \right) \tag{56}$$

is the H_2 norm of the system transfer function from w to z [30]. For the full derivation of this optimization, please refer to [31], [32]. It can be shown that when K is unconstrained, problem (50) and (56) are equivalent, resulting in the same controllers. However, the H_2 problem is more flexible: solving directly for the feedback matrix K, it is possible to enforce constraints in the general form (57) during the optimization.

$$K \in S \tag{57}$$

In this work S has been chosen as

$$S = \begin{bmatrix} \mathbf{0} & K_{afe} & \mathbf{0} \end{bmatrix} \tag{58}$$

where $K_{afe} \in \mathbb{R}^{2\times 3}$ is a control matrix to be found. With this constraint, control action (51) reduces to

$$u = K_{afe} x_{afe} \tag{59}$$

eliminating all the communication problem already described in the presence of a full feedback matrix. The downside of the described approach is that, in general, H_2 optimization problem is non-convex. To overcome non-convexity, a multiple random starting points approach has been used in this paper.

B. NUMERICAL SOLUTION TO THE OPTIMIZATION PROBLEM

The H_2 norm in (56) can be computed as [33]

$$J(K) = \|T_{zw}\|_2 = tr(B_1^T P B_1) \tag{60}$$

where P is the solution of the Lyapunov function

$$(A - B_2K)^T P + P(A - B_2K) = -(Q + K^T R K) \tag{61}$$

The gradient of (60) can be computed as

$$\nabla J(K) = (B_2^T P + RK)\Gamma \tag{62}$$

where Γ is obtained solving the Lyapunov equation

$$(A - B_2K)^T \Gamma + \Gamma(A - B_2K) = B_1 B_1^T \tag{63}$$

The resulting nonlinear programming problem can be solved using some gradient decent based techniques. There are several software solutions available, however, the HIFOO software package [32] was utilised for this study.

C. CONTROLLER TUNING

The controller performance is decided by the weights Q_γ and R_γ. Similar to tuning an LQR controller, the Q_γ matrix penalises the performances of the states. The larger the value for the respective state in Q_γ, the greater the penalisation of the states, and thus the state cannot move much about the equilibrium point, which therefore results in the increase in

TABLE 1. Nominal System Parameters

VSI		AFE	
C	$33\mu F$	C_{dc}	$100\mu F$
R	$65m\Omega$	R_a	$126m\Omega$
L	$227\mu H$	L_a	$566\mu H$
V_{dci}	290V	P_l	$800W$
Reference Values			
$V_{cd_{ref}}$	$100V$	$I_{aq_{ref}}$	0A
$V_{cq_{ref}}$	0V	$V_{L_{ref}}$	400V
$f_{switching}$		10kHz	
f_{sample}		20kHz	
VSI PI Gains			
K_{pv}	0.0261	K_{iv}	10.5526
K_{pi}	1.7321	K_{ii}	7.2589×10^3
PLL Gains			
$K_{P_{pll}}$	2.9995	$K_{I_{pll}}$	636.3961

bandwidth of the controller. As such, the less the Q_γ value on the associated state, the less penalisation and the more the state can move about equilibrium, resulting in reduction in controller bandwidth. On the contrary, the R_γ matrix penalises the inputs. The higher the value in R_γ to the associated input, the more penalisation, and thus the inputs cannot manoeuvrer as freely to return system to equilibrium, resulting in a reduction in bandwidth, and vice versa.

In general, LQR controller tuning involves some trial and error. In the following, a simple tuning procedure is presented in order to attain desired performance. Typically, in systems extended with integral states, Q_γ weights only these states in order to achieve zero steady state error reference tracking, and good disturbance rejection. Therefore, Q_γ is initially set as $Q_\gamma = diag[\,\mathbf{0}^{1\times11}\ 1\ 1\ \mathbf{0}^{1\times2}\,]$. Likewise, the R_γ matrix is initially set as $R_\gamma = \rho I^{2\times2}$, where $\rho = 1$ at the start of the tuning procedure. Firstly, ρ is increased, and the system performances are tested until the response is considered satisfactory; i.e settling times, overshoots/undershoots and controller transient behaviour all being within or close to design limits for given application to which AFE is being installed into. Subsequently, the Q_γ matrix can then be used to fine-tune the weights of the integral states in order to attain the desired performance across each of the states. The system under test has the parameters stated in Table 1, and utlising the above design procedure above for this system, the weights selected were the following:

$$Q_\gamma = diag\left(\left[\mathbf{0}^{1\times11}\quad 0.2\quad 10\quad \mathbf{0}^{1\times2}\right]\right) \tag{64}$$

$$R_\gamma = diag\left(\left[1\ 1\right]\right) \tag{65}$$

D. ADAPTATION FOR OPTIMAL VARIABLE FREQUENCY H_2 CONTROL

The change of system environments often calls for change in controls to ensure that stability and performance can continue to be maintained at optimality. A very common approach to ensure optimality is to gain schedule the controller such that for every possible system operating point, a controller can be selected which ensures the optimal performance of the system. The main issue which arises from gain scheduling is that in some applications, the fastest plant dynamics can be too fast for the controller to keep up with, invalidating the closed loop plant. [34] However, the changing variable in the control plant in this study is the rotational frequency of the grid, which in MEA is directly proportional to the jet engine rotational speed, which typically is a slow transition in the world of controller design. Therefore, the shortcoming of gain-scheduling is unlikely to effect the designed performance of our system and should be fit for purpose. Therefore, to address the changing frequency conditions of the grid into our optimisation, this paper proposes a slight adaptation to the decentralised H_2 control synthesis, in attempting to attain a feedback controller to be interpolated about the grid frequency. As such, our AFE feedback control matrix K_{afe} will be of the form:

$$K_{afe} = \begin{bmatrix} K_{11} & K_{12} & K_{13} & K_{14} & K_{15} \\ K_{21} & K_{22} & K_{23} & K_{24} & K_{25} \end{bmatrix} \tag{66}$$

By cycling the grid frequency ω from $360(2\pi)$ to $800(2\pi)$ rads^{-1}, Fig. 7 shows the variations of some matrix gains, using different number of random starting points in the optimization.

It is clear there is a general smooth polynomial trend arising across all the gains. This figure also shows the importance in the selection of the number of random starting points in the algorithm in order to attain the global minimum of J as well as to have a smooth trend of gains. A polynomial interpolation function as shown in (67) can therefore be used.

$$\hat{K}_{ij}(\omega) = \begin{bmatrix} 1 & \omega & \omega^2 \end{bmatrix} \begin{bmatrix} a_0^{ij} & a_1^{ij} & a_2^{ij} \end{bmatrix}^T \tag{67}$$

where the coefficients a_0^{ij}, a_1^{ij} and a_2^{ij} have been obtained using a Least Square method.

Since the interpolated controller is optimised adhering to the structure imposed by (58), each of the columns in K_{afe} actuates a given state, as per (59). Therefore, K_{afe} can be split further down into a proportional controller $K_p^{2\times3}(\omega)$ which acts directly on the AFE states, and an integral controller $K_i^{2\times2}(\omega)$ which acts on the integral states of the controller, such that the controller can be represented as:

$$K_{afe}(\omega) = \begin{bmatrix} K_p(\omega) & K_i(\omega) \end{bmatrix} \tag{68}$$

Therefore, the control law from (59) can be separated further into:

$$\begin{bmatrix} p_d \\ p_q \end{bmatrix} = K_p(\omega) \begin{bmatrix} I_{ad} \\ I_{aq} \\ V_L \end{bmatrix} + K_i(\omega) \begin{bmatrix} \chi_{I_{aq}} \\ \chi_{V_L} \end{bmatrix} \tag{69}$$

where

$$\chi_{I_{aq}} = \int (I_{aq_{ref}} - I_{aq}) \tag{70}$$

$$\chi_{V_L} = \int (V_{L_{ref}} - V_L) \tag{71}$$

From this, the proposed AFE controller implementation is presented in Fig. 6.

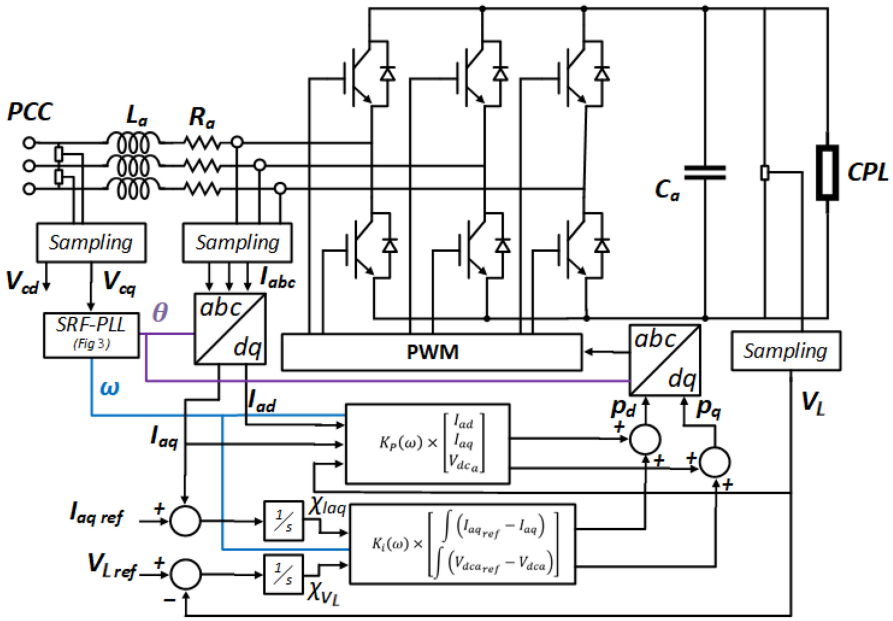

FIGURE 6. Controller block diagram of the proposed optimal H_2 control with frequency gain scheduling. Additionally this is the same scheme incorporated for the LQR controller during testing.

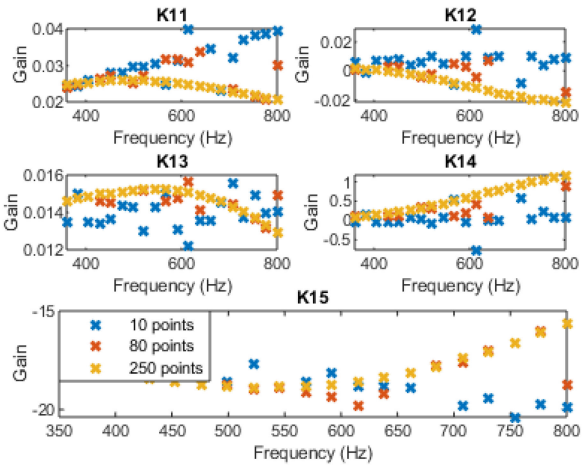

FIGURE 7. Variation in the value of each gain with frequency, for varying random starting point values for H_2 optimization.

V. EXPERIMENTAL RESULTS AND PERFORMANCE ANALYSIS

A. EXPERIMENTAL TEST RIG AND TEST CONDITIONS

The proposed controller shall be compared to a PI and a standalone LQR controller. The LQR controller shall be designed considering the AFE dynamics only. To maintain good and fair performance comparison across the controllers, they are each tuned to the fastest bandwidth possible on the experimental setup. The PI controller for the AFE has been designed to 900 Hz for the inner current loop, and 90 Hz for the outer voltage loop, with use of the design procedure described in [35]. The LQR is tuned in order to be comparable in dynamic performance to that of the H_2 designed in Section IV-C, and using the same tuning procedures, Q_γ for the LQR controller was selected as:

$$Q_{lqr} = 60diag\left(\begin{bmatrix} 0 & 0 & 0 & 1 & 4 \end{bmatrix}\right) \tag{72}$$

whilst R_γ was selected to be that defined in (65).

Due to the PI controller transfer functions not being dependant on frequency as shown in [35], a polynomial gain adaptation is not required for the PI. However, since the LQR control is similar in form to the H_2 controller, it is dependant on frequency, and therefore the LQR has also been adapted for variable frequency using the same procedure for the H_2 controller, as described in Section IV-D.

Each of these controllers have been implemented onto an experimental test rig consisting of commercial converters, with the VSI being a 2 kW, 300 V converter from BMT (Best Motion Technologies), and the AFE is a 3 kW converter from Semicron, with the setup shown in Fig. 8. The parameters of the test rig, as well as the control references used, the VSI PI controller, and AFE PLL gains are all detailed in Table 1.

B. EXPERIMENTAL ANALYSIS

Two tests are presented in this paper to analyze performance of the proposed controller. The first test applies a 800 W step load during grid frequency transient, to analyze both low frequency dynamic performance, and frequency transient performance. Its results are shown in Fig. 9. From analyzing the performance of the frequency transient after the step load disturbance, good tracking and steady state performance for the system can be observed, with each controller easily able to handle the dynamics of the frequency ramp. This shows the adaptation to the controller design in Sec IV-D ensures good

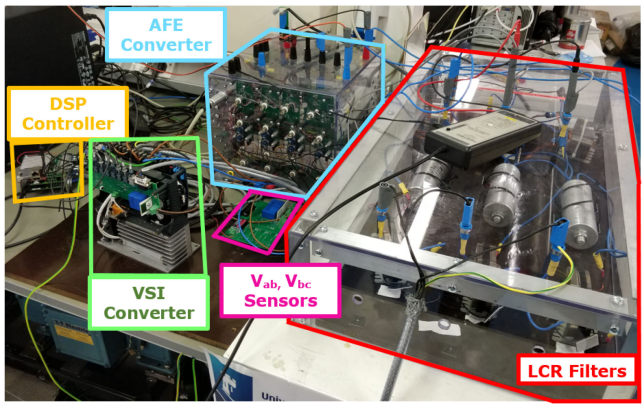

FIGURE 8. Experimental rig setup.

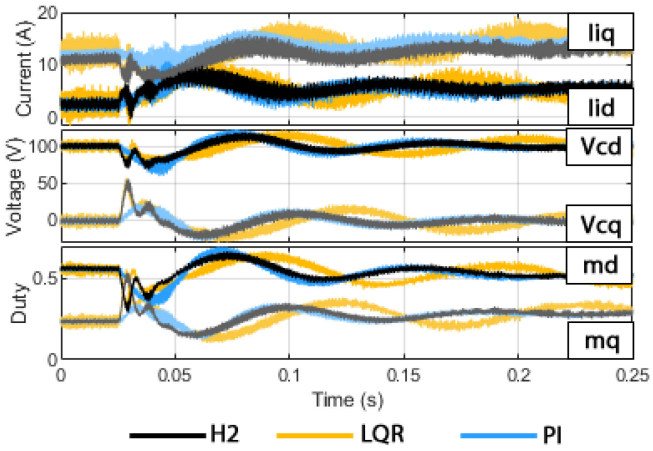

(a) VSI states: Iid/q (Top), Vcd/q (Middle) and md/q (Bottom)

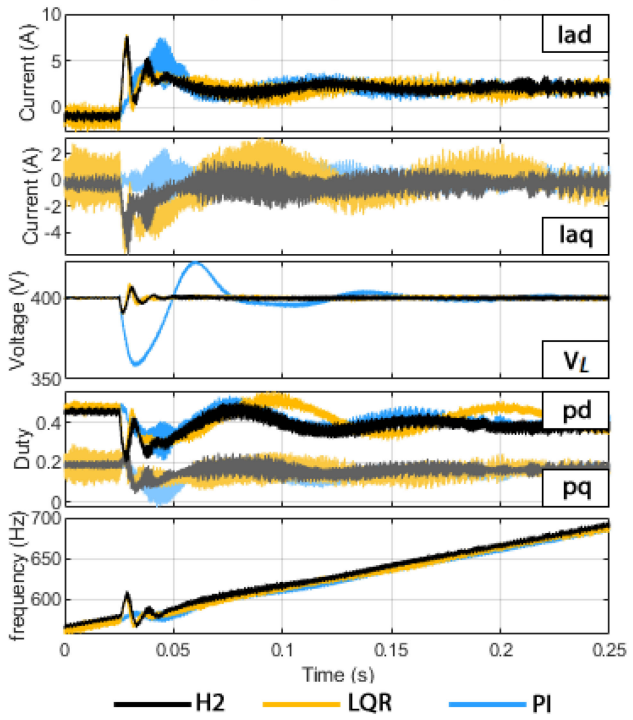

(b) AFE states, including PLL frequency tracking

FIGURE 9. 360–800 Hz frequency ramp with 0.8 kW step load.

performance across all frequencies for the optimal controls. Analyzing the performance at the point of the load step, both LQR and the proposed H_2 controller improve the dynamic performance on the AFE states I_{ad} and V_L. Both controls exhibit a 75% improvement in overshoot attenuation and 40% increase to dynamic speed for V_L when compared to PI. Both the optimal controllers show faster suppression to overshoots in I_{ad}, and gets within steady-state values approximately 50% faster than compared with PI controls. I_{aq} is the only state which results in worse performance that PI, with overshoots of upto 5 A, compared to about 1 A exhibited with PI. This comes largely as a result of how the state bandwidths for both the LQR and H_2 controllers are configured, and the fact that with every significant improvement, there is always a drawback, where the deteriorated performance of I_{aq} is the drawback of the optimal controller design.

Upon analysing (64) and (72), it can be seen that the V_L integral state is greatly weighted with respect to I_{aq} integral state, thus resulting in a much faster bandwidth for V_L state. However, when tuning the system in an attempt to reduce the difference in the weights between I_{aq} and V_L it was found that for a small improvement in the I_{aq} dynamic, the dynamic of V_L significantly deteriorated. Therefore, since aircraft regulations are more stringent on maintaining DC-Link voltage performance over the current, the voltage bandwidth was prioritized, and the deterioration of I_{aq} is seen as a drawback to adopting optimal controllers compared to PI controls.

The second test analyzes static 800 Hz frequency step load response. Its results in Fig. 10 highlights the advantages received when adopting our decentralized H_2 controller approach. As seen from the first test, due to no frequency dependence of the PI controller definitions, the PI performs much the same as at lower frequencies, whilst H_2 shows minute performance increase. Most evidently in I_{aq} where the undershoot is decreased by 3 A in comparison to at low frequencies. This is likely down to how the closed loop performance of the controller changes over the range of operable frequencies. As the system operates across the full range of frequencies, the dynamics described in the A matirx (37) in turn changes, and therefore so does the close loop performance of the system. As can be seen from Fig. 11, the closed loop dominant pole bandwidths of that at around 360 Hz is slower than that at 800 Hz, and therefore performance increase of the overall controller is to be expected. This can explain why improved performance of I_{aq} is attained at 800 Hz.

Analysing the performance of the VSI converter, it can be observed that the system involving the H_2 controller allows the VSI to operate as designed by it's PI controller, since almost identical performance is attained between PI and H_2 experiments for the VSI states. This is down largely to the fact that the H_2 controller is optimized around the closed loop performance of the VSI PI controller, and thus less interactions between the two controllers is observed. The LQR system on the other hand, shows a more oscillatory dynamic across all system states after the disturbance, as a result of controller interaction between AFE and VSI. To explain this, consider

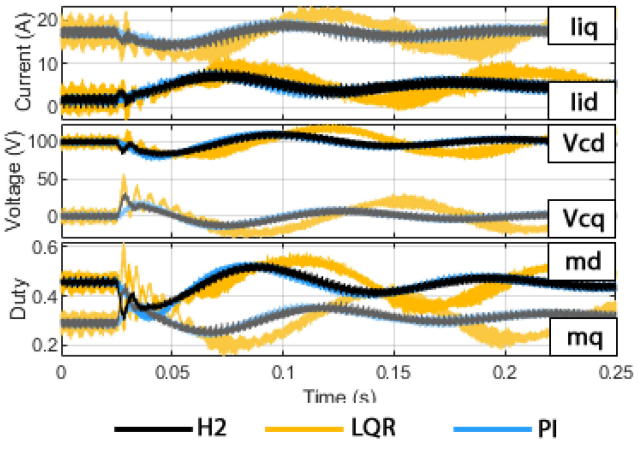

(a) VSI Terms: Iid/q (Top), Vcd/q (Middle) and md/q (Bottom)

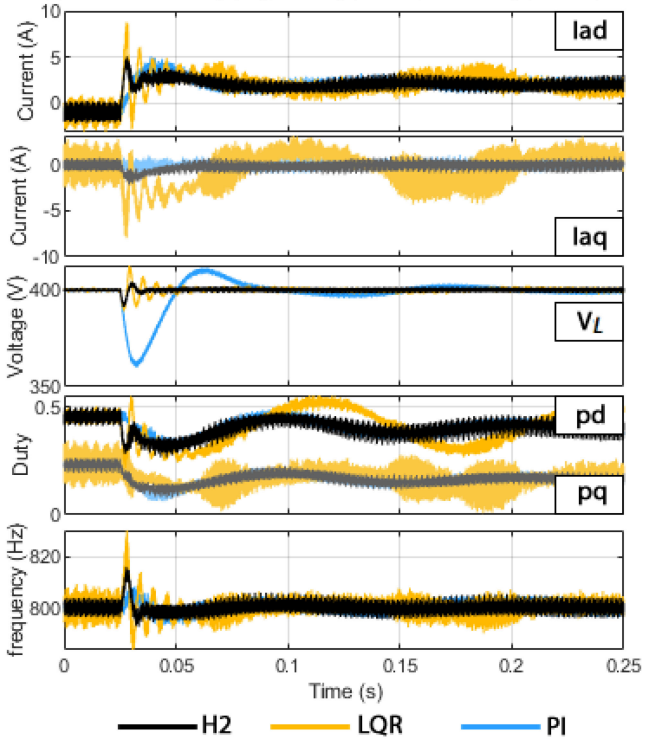

(b) AFE states, including PLL frequency tracking

FIGURE 10. 800 Hz steady state 0.8 kW step load test.

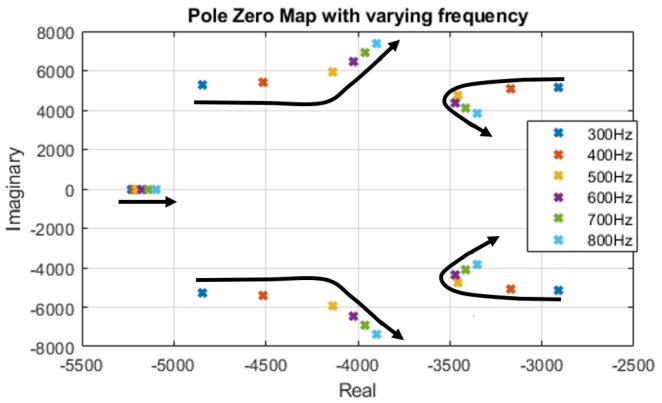

FIGURE 11. Pole-zero map of the closed loop H_2 controlled AFE System as grid frequency is varied.

how each, the proposed H_2 and the LQR are synthesised. With our proposed approach, each of the gains synthesised at each of the frequencies to develop $K(\omega)$ accounts for the change in closed loop dynamics due to frequency of both the VSI and AFE, via the global model (37) used to synthesis the controller. Therefore, each of the polynomial gains in $K(\omega)$ for H_2 is optimised with the knowledge of the interactive effects between the converters, and the change in each of their dynamics due to changing operating frequency. The LQR however is optimised locally, and doesn't account for any dynamic changes which occurs on the VSI, or any the interactive effects with the AFE. As the dynamics of the VSI change as frequency increases, these unaccounted interactive effects can cause further detriment to the controller, as observed with the oscillatory response from the LQR. As such, the results have shown the advantages from our proposed method in guaranteeing global stability and robustness of the grid when installing new converters onto a network, whilst also allowing for optimal performance across fast varying variable frequency power systems.

In addition, the proposed controller implementation was programmed onto a TMS320F6713 DSP utilising the *uCube* controller as described in [36]. The execution time for the controller was found to be 6.3 μs, which entails minimal computational burden on the control platform.

C. SUMMARY OF OBSERVATIONS

In summary of all the experimental analyses presented, it is clear that for the most part, the PI controller is still the easier of the presented options for implementation. The PI transfer functions are not grid frequency dependant which allows straight forward design of the its gains, with the knowledge it will work across the full range of operable frequencies of the system. However, it is clear for the PI controller that due to the fact that each controller in designed about the local converter transfer functions, without consideration to the global dynamics of the grid, state interactions can occur. Especially so in the V_L state, and one could expect this detriment in performance to worsen, as filter size reduces. For the LQR and H_2 controllers, it was shown that both systems are grid-frequency dependant, and to ensure that the controller remains optimum for full operational range of grid frequencies, interpolated gain scheduling is required, which does increase the complexity of the implementation somewhat. For the LQR however, problems ensue due to the fact that the resultant LQR controller cannot be structured. This therefore means that the LQR controller can only be optimised about the local dynamics of the AFE instead of being optimised about the global grid dynamics, if one wishes to keep a decentralised controller implementation for the grid. As such, the changing dynamics of the VSI with frequency cannot be appropriately accounted for. This, as was

observed for the PI caused interactions to occur between converters, even resulting in some oscillatory behaviour to occur on load transients which is highly undesirable. Additionally, an interesting thing to note from the results of both Fig. 9 and Fig. 10 is the VSI dynamic when LQR control is utilised on the AFE. Comparing against the PI and H_2 controls, it becomes quite evident, that the LQR control seems to slow down the overall performance of the VSI states. Oscillations appear prolonged and in the case of the currents, appear to increase in amplitude. It therefore shows, the uncharacterised interactions in the LQR control appears to cuase the effect of slowing down the dynamic performance of the VSI.

The H_2, unlike LQR can have its output controller K structured. This allows for the global model of the grid to be submitted for optimisation, whilst outputting only AFE gains. Therefore, unlike what could have been performed for the LQR controller, as the system changes in frequency, the interpolated gains of the H_2 controller are optimised accounting for the changing closed loop dynamics of the VSI. As such, from the results, the H_2 controller was shown to not only improve the dynamic performance for the majority of AFE states, but allowed the VSI to operate as had been designed. Therefore, the proposed H_2 controller allows for significant improvements in dynamic performance for the AFE; it allows for optimal performance of the grid to be achieved across the full operating frequency range of the electrical system, and mitigates against dynamic cross-interactions between converters, therefore allowing the VSI to operate as designed, and the AFE to operate with improved dynamic performance over traditional designs of controller.

VI. CONCLUSION

This paper presents an approach for designing a globally optimal decentralised controller for an individual grid-tied converter being installed into a pre-designed variable frequency aircraft power electronic embedded grid. Due to the ability of the proposed H_2 controller design allowing for the characterisation of the closed loop dynamics of the global system to which the AFE will be installed into, the proposal offered many advantages. This ability allowed the development of an independent regulator to be designed which is optimal to the rest of the grid in which this AFE will be installed into. A more traditional approach to optimal controller design in these applications would have likely been the LQR controller, which due to its inability to develop structured controllers, would result in locally optimised converters around the individual target converter dynamics. Whilst the implementation of an LQR controller did show significant improvement to converter performance over traditional cascade PI controllers, when it was compared against the proposed globally decentralised H_2 controller, the weaknesses of the LQR controller did become evident. Since the proposed approach considers the closed loop dynamics of the grid, as well as the cross-converter interactions in the optimisation, the H_2 controller shows significant dynamic performance increases across nearly all AFE states, as well as vitally allowing the rest of the grid to operate as was designed with little interactive effects.

In addition, this paper introduced a gain-scheduling approach for the proposed controller, enabling the development of a variable frequency decentralised optimal controller. It is shown to be a simple implementation, and has shown to deliver excellent performance across the full frequency range, maintaining desired performance throughout. This method was also applied to the LQR control, however, due to the LQR being unable to be optimised with respect to the changing grid dynamics with frequency, exhibited even greater oscillatory interactions with the rest of the system. An improved method of development of independent optimal controllers for grid-tied converters, with a low computation burden on the control platform has therefore been shown, and in future work, this shall be shown to be applied for expanded system, where multiple converters maybe installed at once.

REFERENCES

[1] P. Wheeler, "Technology for the more and all electric aircraft of the future," in *Proc. IEEE Int. Conf. Automat.*, 2016, pp. 1–5.

[2] B. Sarlioglu and C. T. Morris, "More electric aircraft: Review, challenges, and opportunities for commercial transport aircraft," *IEEE Trans. Transp. Electrific.*, vol. 1, no. 1, pp. 54–64, Jun. 2015.

[3] P. Zanchetta, M. Degano, J. Liu, and P. Mattavelli, "Iterative learning control with variable sampling frequency for current control of grid-connected converters in aircraft power systems," *IEEE Trans. Ind. Appl.*, vol. 49, no. 4, pp. 1548–1555, Jul./Aug. 2013.

[4] Z. Zhang, J. Li, Y. Liu, Y. Xu, and Y. Yan, "Overview and development of variable frequency ac generators for more electric aircraft generation system," *Chin. J. Elect. Eng.*, vol. 3, no. 2, pp. 32–40, 2017.

[5] J. A. Rohten *et al.*, "Enhanced predictive control for a wide time-variant frequency environment," *IEEE Trans. Ind. Electron.*, vol. 63, no. 9, pp. 5827–5837, Sep. 2016.

[6] K. Areerak, S. Bozhko, G. Asher, L. De Lillo, and D. W. Thomas, "Stability study for a hybrid ac-dc more-electric aircraft power system," *IEEE Trans. Aerosp. Electron. Syst.*, vol. 48, no. 1, pp. 329–347, Jan. 2012.

[7] J. Benzaquen, M. B. Shadmand, and B. Mirafzal, "Ultrafast rectifier for variable-frequency applications," *IEEE Access*, vol. 7, pp. 9903–9911, 2019.

[8] J.-L. Schanen, A. Baraston, M. Delhommais, P. Zanchetta, and D. Boroyevitch, "Sizing of power electronics emc filters using design by optimization methodology," in *Proc. 7th Power Electron. Drive Syst. Technol. Conf.*, 2016, pp. 279–284.

[9] T. Roinila *et al.*, "Hardware-in-the-loop methods for real-time frequency-response measurements of on-board power distribution systems," *IEEE Trans. Ind. Electron.*, vol. 66, no. 7, pp. 5769–5777, Jul. 2019.

[10] M. Kim, S. G. Lee, and S. Bae, "Decentralized power management for electrical power systems in more electric aircrafts," *Electronics*, vol. 7, no. 9, 2018.

[11] Z. Cheng, J. Duan, and M.-Y. Chow, "To centralize or to distribute: That is the question: A comparison of advanced microgrid management systems," *IEEE Ind. Electron. Mag.*, vol. 12, no. 1, pp. 6–24, Mar. 2018.

[12] A. R. Messina, O. Begovich, J. López, and E. Reyes, "Design of multiple facts controllers for damping inter-area oscillations: A decentralised control approach," *Int. J. Elect. Power Energy Syst.*, vol. 26, no. 1, pp. 19–29, 2004.

[13] M. Jayachandran and G. Ravi, "Decentralized model predictive hierarchical control strategy for islanded ac microgrids," *Elect. Power Syst. Res.*, vol. 170, pp. 92–100, 2019.

[14] P. Falkowski and A. Sikorski, "Finite control set model predictive control for grid-connected ac–dc converters with LCL filter," *IEEE Trans. Ind. Electron.*, vol. 65, no. 4, pp. 2844–2852, Apr. 2018.

[15] X. Zhang, L. Tan, J. Xian, H. Zhang, Z. Ma, and J. Kang, "Direct grid-side current model predictive control for grid-connected inverter with LCL filter," *IET Power Electron.*, vol. 11, no. 15, pp. 2450–2460, 2018.

[16] A. Formentini, D. Dewar, P. Zanchetta, P. Wheeler, D. Boroyevich, and J.-L. Schanen, "Optimal control of three-phase embedded power grids," in *Proc. IEEE 17th Workshop Control Model. Power Electron.*, 2016, pp. 1–6.
[17] B. R. Vellaboyana and J. A. Taylor, "Optimal decentralized control of dc-segmented power systems," *IEEE Trans. Automat. Control*, vol. 63, no. 10, pp. 3616–3622, Oct. 2018.
[18] X. Wu, F. Dörfler, and M. R. Jovanović, "Input-output analysis and decentralized optimal control of inter-area oscillations in power systems," *IEEE Trans. Power Syst.*, vol. 31, no. 3, pp. 2434–2444, May 2016.
[19] L. Bakule, "Decentralized control: An overview," *Annu. Rev. Control*, vol. 32, no. 1, pp. 87–98, 2008.
[20] D. Dewar, A. Formentini, and P. Zanchetta, "Automated and scalable optimal control of three-phase embedded power grids including PLL," in *Proc. IEEE Energy Convers. Congr. Expo.*, 2017, pp. 4252–4259.
[21] K. Li, D. Dewar, A. Formentini, P. Zanchetta, and P. Wheeler, "Grid impedance identification and structured-H2 optimization based controller design of active front-end in embedded ac networks," in *Proc. IEEE Energy Convers. Congr. Expo.*, 2019, pp. 4840–4845.
[22] D. Dewar, J. Rohten, A. Formentini, and P. Zanchetta, "Fast self-tuning decentralized variable frequency optimal controller design for three-phase embedded grids," in *Proc. IECON 45th Annu. Conf. IEEE Ind. Electron. Soc.*, 2019, pp. 3894–3899.
[23] T. Tarczewski and L. M. Grzesiak, "State feedback control of the pmsm servo-drive with sinusoidal voltage source inverter," in *Proc. 15th Int. Power Electron. Motion Control Conf.*, 2012, pp. DS2a–6.
[24] Y. Huangfu, S. Pang, B. Nahid-Mobarakeh, L. Guo, A. K. Rathore, and F. Gao, "Stability analysis and active stabilization of on-board dc power converter system with input filter," *IEEE Trans. Ind. Electron.*, vol. 65, no. 1, pp. 790–799, Jan. 2018.
[25] S. Hiti, D. Boroyevich, and C. Cuadros, "Small-signal modeling and control of three-phase PWM converters," in *Proc. IEEE Ind. Appl. Soc. Annu. Meeting.*, 1994, pp. 1143–1150.
[26] B. Wen, D. Boroyevich, R. Burgos, P. Mattavelli, and Z. Shen, "Analysis of dq small-signal impedance of grid-tied inverters," *IEEE Trans. Power Electron.*, vol. 31, no. 1, pp. 675–687, Jan. 2016.
[27] J. Sawma, F. Khatounian, E. Monmasson, L. Idkhajine, and R. Ghosn, "Cascaded dual-model-predictive control of an active front-end rectifier," *IEEE Trans. Ind. Electron.*, vol. 63, no. 7, pp. 4604–4614, Jul. 2016.
[28] Q. Li *et al.*, "Taking into account interactions between converters in the design of aircraft power networks," in *Proc. IEEE Energy Convers. Congr. Expo.*, 2016, pp. 1–7.
[29] S. Skogestad and I. Postlethwaite, *Multivariable Feedback Control: Analysis and Design*. Hoboken, NJ, USA: Wiley, 2007, vol. 2.
[30] A. A. Moelja and G. Meinsma, "H2 control of preview systems," *Automatica*, vol. 42, no. 6, pp. 945–952, 2006.
[31] M. Athans and P. L. Falb, *Optimal Control: An Introduction to the Theory and its Applications*. Courier Corporation, 2013.
[32] D. Arzelier, D. Georgia, S. Gumussoy, and D. Henrion, "H2 for hifoo," 2010, *arXiv:1010.1442*.
[33] F. Lin, M. Fardad, and M. R. Jovanovic, "Augmented lagrangian approach to design of structured optimal state feedback gains," *IEEE Trans. Automat. Control*, vol. 56, no. 12, pp. 2923–2929, Dec. 2011.
[34] G. Ellis, *Control System Design Guide: Using your Computer to Understand and Diagnose Feedback Controllers*. Butterworth-Heinemann, 2012.
[35] D. Dewar, K. Li, A. Formentini, P. Zanchetta, and P. Wheeler, "Performance analysis of *h*_{2} optimally controlled three-phase grids," in *Proc. IEEE Energy Convers. Congr. Expo.*, 2018, pp. 2258–2264.
[36] A. Galassini, G. L. Calzo, A. Formentini, C. Gerada, P. Zanchetta, and A. Costabeber, "ucube: Control platform for power electronics," in *Proc. IEEE Workshop Elect. Mach. Des., Control Diagnosis.*, 2017, pp. 216–221.

DAVID DEWAR (Student Member, IEEE) received the M.Eng. (Hons.) degree in 2016 in electrical and electronic engineering from the University of Nottingham, Nottingham, U.K., where he is currently working toward the Ph.D. degree in electrical engineering. His Doctoral and current research interests include microgrids, decentralized optimal controller design, and grid optimization techniques.

JAIME ROHTEN (Member, IEEE) received the B.E. (Hons.) degree in electronic engineering, and the M.Sc. and D.Sc. degrees in electrical engineering from the University of Concepcion, Concepcion, Chile, in 2010, 2012, and 2017, respectively. Since 2015, he has been teaching in the areas of power electronic and control systems analysis with the Department of Electrical and Electronic Engineering, Universidad del Bío-Bío, Concepción, Chile. His research interests include hydrogen storage system, renewable energies, digital nonlinear, resonant, and predictive control for voltage or current source converters.

ANDREA FORMENTINI (Member, IEEE) received the M.S. degree in computer engineering and the Ph.D. degree in electrical engineering from the University of Genova, Genova, Italy, in 2010 and 2014, respectively. He then joined as Research Fellow with the Power Electronics, Machines and Control Group, University of Nottingham, Nottingham, U.K. Since 2018, he has been an Assistant Professor with the University of Nottingham. His research interests include control of electrical machine drives and power converters.

PERICLE ZANCHETTA (Fellow, IEEE) received the M.Eng. degree in electronic engineering and the Ph.D. degree in electrical engineering from the Technical University of Bari, Bari, Italy, in 1993 and 1997, respectively. In 1998, he became an Assistant Professor of power electronics with the Technical University of Bari. In 2001, he became a Lecturer in control of power electronics systems with the PEMC Research Group, University of Nottingham, where he is currently a Professor in control of power electronics systems. He is also a part-time Professor with the University of Pavia, Pavia, Italy. He has authored or coauthored more than 350 peerreviewed papers. His research interests include control and optimization of power converters and drives, Matrix, and multilevel converters. He was the Chair of the IEEE-IAS Industrial Power Converter Committee IPCC from 2016 to 2017 the IEEE-IAS Industrial Power Conversion Systems Department IPCSD 2020–2021, and the Transactions Review Chair for IPCC from 2018 to 2021.